

Ultrasonic imaging of concrete using Wavelet transform and Hilbert-Huang transform as signal processing tools

Oscar Victor M. Antonio, Jr.* and Sohichi Hirose**

*Graduate Student of Tokyo Institute of Technology (Ookayama, Meguro-ku, Tokyo 152-8550)

**Professor of Tokyo Institute of Technology (Ookayama, Meguro-ku, Tokyo 152-8550)

In ultrasonic NDE for concrete, accurate images are difficult to obtain since the grain size distribution is highly variable and the properties of the constituent materials are greatly varied. In this paper, signal processing methods such as Discrete Wavelet Transform (DWT), Wavelet Packet Transform (WPT) and the Hilbert-Huang Transform (HHT) were used to analyze the ultrasonic waveforms taken from a concrete specimen with an embedded steel rod. Synthetic Aperture Focusing Technique (SAFT) images for both processed and unprocessed signals were obtained and compared. Results showed that the concrete bottom surface and the steel rod were successfully imaged using the WPT-HHT for processing the waveforms. Therefore, anomaly or defect detection in concrete structures through ultrasonic imaging was greatly improved by the combination of WPT-HHT and SAFT.

Key Words: *ultrasonic imaging, signal processing, Wavelet transform, Hilbert-Huang transform*

1. Introduction

For non-destructive evaluation (NDE) of concrete, efficient and accurate imaging techniques are needed for a reliable evaluation of safety and serviceability of structures. Imaging of concrete structures for non-destructive testing purposes is defined in a broad sense as obtaining a representation of certain physical properties of concrete material and characteristics of the physical system by indirect or remote sensing methods which will not damage the structure, or permanently impair its serviceability¹⁾. Since concrete is a highly non-homogeneous material, imaging of concrete structures is considered a very challenging task. Most of the time concrete is produced in the field with very limited quality control. Also, grain size distribution is highly variable and the properties of the constituent materials are greatly varied making it difficult to obtain accurate images. At present, there are several techniques used for imaging concrete structures. These include X-ray and gamma-ray radiography, computerized radioactive tomography based on X-rays and gamma-rays, infrared thermography, radar (microwave) and acoustic (stress wave) techniques. In this paper, the acoustic (stress wave) technique is applied by using Ultrasonics and Synthetic Aperture Focusing Technique (SAFT). An ultrasonic pulse is generated by

exciting a piezoelectric material with a high-amplitude, transient electrical pulse from a high-voltage, and high current pulser. The short burst of ultrasonic energy is transmitted into the concrete and impinges upon various interfaces within the concrete. The change in acoustic impedance at the various interfaces such as air voids, water-filled voids, soil-intrusion, reinforcing bars, cracks, delaminations and other interfaces or inclusions within the concrete causes some portions of the input energy to reflect or echo back to the surface²⁾. These energy reflections are then received and converted back to electrical pulse as waveform data. However, these received waveforms are usually difficult to interpret and the resulting images may lead to wrong evaluation. Moreover, the presence of coarse aggregate, often exceeding 10 millimeters in diameter, requires that ultrasonic testing in concrete be conducted at relatively low frequencies in order to avoid excessive attenuation caused by scattering¹⁾.

In concrete ultrasonic testing, particularly for indirect transmission tests, the resulting waveforms almost always characterized by several oscillations (multi-mode arrival times) due to the reflections from various scatterers within the concrete. Reflections from these multiple scatterers make the interpretation of the waveform very difficult or sometimes make it meaningless. Thus, digital signal processing (DSP) is needed in order to aid in the interpretation of these waveforms. Signal processing is based

on transforming the signal or waveform in a manner that is more useful to the application at hand³⁾. Specifically, signal processing is used to decompose the waveforms into its simple oscillatory components and to eliminate noise or any unnecessary components. Also, signal processing is very important to time-frequency analysis for better understanding and interpretation of the waveforms as well as the resulting images. It should be noted that to create better and meaningful images, the received waveforms should be subjected to signal processing prior to the application of Synthetic Aperture Focusing Technique. Two relatively new signal processing techniques were considered in this paper: Wavelet Transform (WT) and Hilbert-Huang Transform (HHT). WT has a complete theoretical foundation while HHT is semi-empirically based. These signal processing methods as well as the imaging technique, SAFT, will be discussed in the following subsections.

1.1 Wavelet transform

Wavelet is defined as a localized wave of effectively limited duration (finite energy), has an average value of zero and it is used to represent signals. Unlike previous methods used for modeling complex signals, wavelets can be used to model non-stationary signals. Wavelet analysis is a relatively new method, though its mathematical foundation dates back to the work of Joseph Fourier in the nineteenth century. The concept of wavelets in its present theoretical form was first proposed mainly by Jean Morlet and the team at Marseille Theoretical Physics Center working under Alex Grossman in France⁴⁾.

Wavelet transform, in general, is the representation of a function by wavelets. The wavelets are scaled and translated versions (daughter wavelets) of a finite-length or fast-decaying oscillating waveform (mother wavelet). Wavelet analysis consists of decomposing a signal into hierarchical set of Approximations (A) and Details (D). The approximation is defined as the high scale, low frequency components of the signal while the detail is the low scale, high frequency components.

Wavelet transform of a signal does not change the information contained in the signal, it is just a different representation of the signal. There are two general types of wavelet transform, Continuous Wavelet Transform (CWT) and Discrete Wavelet Transform (DWT). Mathematically, wavelet transform maps a function, $x(t)$, into a two-dimensional domain (time-scale plane) and is denoted by $W(a,b)$ given by

$$W(a,b) = \frac{1}{\sqrt{a}} \int_{-\infty}^{+\infty} x(t) \psi^* \left(\frac{t-b}{a} \right) dt \quad (1)$$

$$= \int_{-\infty}^{+\infty} x(t) \psi_{ab}^* (t) dt$$

where $\psi(t)$ is called the mother wavelet, which is a continuous function in both the time domain and the frequency domain and the * represents operation of complex conjugate. The main purpose of the mother wavelet is to provide a basis function of

the transform, called daughter wavelets, given by

$$\psi_{ab} = \frac{1}{\sqrt{a}} \psi \left(\frac{t-b}{a} \right). \quad (2)$$

$\psi_{ab}(t)$ is a set of basis functions obtained from the mother wavelet $\psi(t)$ by dilation or compression using scaling parameter a and temporal translation using shift parameter b . The scaling parameter a is positive and varies from 0 to ∞ . For $a < 1$, the transform performs compression while for $a > 1$, the transform performs dilation of the signal.

The signal $x(t)$ can be recovered from the wavelet coefficients $W(a,b)$ by the Inverse Wavelet transform given by:

$$x(t) = \frac{1}{c} \int_{-\infty}^{+\infty} \int_0^{+\infty} \frac{1}{a^2} W(a,b) \psi \left(\frac{t-b}{a} \right) da db \quad (3)$$

provided that the constant c is

$$c = \int_{-\infty}^{+\infty} \frac{|\psi(\omega)|^2}{\omega} d\omega < \infty \quad (4)$$

where $\psi(\omega)$ is the Fourier transform of the mother wavelet. Eq. (4) is generally known as the admissibility formula⁵⁾.

The general algorithm in performing Wavelet transform is briefly described by the following steps:

- 1) Choose a wavelet and compare it to a section at the start of the original signal.
- 2) Calculate the coefficient, W , which represents how closely related the wavelet with this section of the original signal.
- 3) Translate or Shift the wavelet to the right and repeat steps 1) and 2) until the whole signal is covered.
- 4) Scale (dilate or compress) the wavelet and repeat steps 1) through 3).
- 5) Repeat steps 1) through 4) for all scales.

The difference between CWT and DWT is the set of scales and positions at which they operate. Continuous wavelet transform can operate at every scale, from one up to some specified scale value. Also, the analyzing wavelet is shifted smoothly over the full domain of the analyzed function. Unlike the continuous wavelet transform, the DWT uses subset of scales and positions based on the powers of two (dyadic scale). Moreover, DWT requires less computational horsepower but is just as accurate as CWT.

On the other hand, Wavelet Packet analysis method is a generalization of the wavelet decomposition which offers a wider range of possibilities for the signal analysis⁴⁾. In the usual wavelet analysis, a signal is decomposed into an approximation and a detail. The approximation is then decomposed into a second level approximation and detail, and the process is repeated until the desired decomposition level is reached. In wavelet packet analysis, the approximations as well as the details are decomposed at each level. Fig. 1 shows the third level decomposition tree for both wavelet analysis and wavelet packet analysis.

Fig. 1(a)

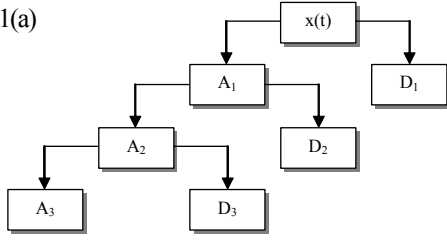


Fig. 1(b)

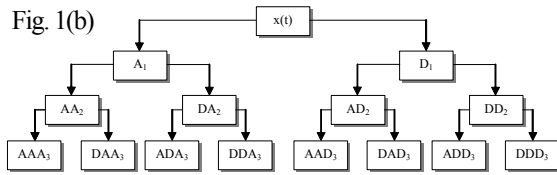


Fig. 1 Third level decomposition tree.

(a) Wavelet Analysis, (b) Wavelet Packet Analysis

1.2 Hilbert-Huang transform

The Hilbert-Huang Transform, also known as HHT, is an empirically-based adaptive data-analysis method developed by Huang *et al.*⁶⁾. Its development was motivated by the need to describe in detail the nonlinear distorted waves. Being adaptive means that the definition of the basis function has to be data-dependent, an *a posteriori*-defined basis, an approach totally different from the established mathematical paradigm for data analysis. Its algorithm consists of two parts: Mode Decomposition (MD) and Hilbert Spectral Analysis (HSA). HHT method is potentially viable for nonlinear and non-stationary data analysis, especially for time-frequency-energy representations. It has been tested and validated exhaustively, but only empirically⁷⁾.

The mode decomposition part serves as a filter that sifts through the data and breaks it down into simpler components called Intrinsic Mode Function (IMF). The sifting operation involves getting the mean envelope from the upper and lower envelopes of the original dataset and then subtracting it from the original dataset. An IMF is produced if the number of extrema differs from the number of zero crossings by not more than one and the mean value of the envelopes is zero. The data returned as IMF is stored and subtracted from the parent data. The difference is then used as a parent dataset for a new sifting process and the procedure is repeated until the residue becomes a monotonic function, from which no more IMF can be extracted. After obtaining all the IMFs, the HSA procedure is applied to each IMF to obtain the instantaneous frequency and consequently the frequency-energy distribution as a function of time. Described below is the detailed algorithm in performing the HHT.

(1) Empirical mode decomposition

Empirical mode decomposition (EMD) is a sifting process to decompose the waveform data into its intrinsic modes. The decomposition is based on the assumption that any data consists of different intrinsic modes of oscillations. Each intrinsic mode, linear or nonlinear, represents a simple oscillation. At any given time, the data may have many different coexisting modes of oscillation, one superimposing on the others. As a result, the waveform appears to be complicated. Each of these simple oscillatory modes is represented by an intrinsic mode function (IMF) with the following characteristics:

- (1) in the whole dataset, the number of extrema and the number of zero-crossings must either be equal or differ at most by one, and
- (2) at any point, the mean value of the envelope defined by the local maxima and the envelope defined by the local minima is zero.

IMF represents a simple oscillatory mode as a counterpart to the simple harmonic function, but it is much more general: instead of constant amplitude and frequency, as in a simple harmonic component, the IMF can have variable amplitude and frequency as a function of time. The total number of IMF components is close to $\log_2 N$, where N is the total number of data points⁷⁾.

The sifting process for a given data $x(t)$ is as follows: First, identify the local extrema (maxima and minima) and then obtain the upper and lower envelopes by connecting the local maxima and local minima using cubic spline method, respectively. Their mean is designated as m_l , and the difference between the data and m_l is the first component h_l , which is a candidate for IMF,

$$h_1 = x(t) - m_1. \quad (5)$$

Ideally, h_l should satisfy the definition of an IMF, the procedure should have made it symmetric and have all maxima positive and all minima negative. However, even if the sifting procedure is perfect, a gentle hump on a slope can be amplified to become a local extremum in changing the local zero from rectangular to a curvilinear coordinate system. The sifting process serves two purposes: 1) to eliminate the riding waves; and 2) to make the wave profiles more symmetric. While the first purpose must be achieved for the Hilbert Transform to give a meaningful instantaneous frequency, the second purpose must also be achieved in case the neighboring wave amplitudes have too large disparity⁷⁾. The sifting process has to be repeated as many times as it is required to reduce the extracted signal to an IMF. In the subsequent sifting processes, h_1 is treated as the data for the next round of sifting. After repeating the sifting process k number of times, h_{1k} is obtained

$$\begin{aligned}
h_{11} &= h_1 - m_{11} \\
h_{12} &= h_{11} - m_{12} \\
h_{13} &= h_{12} - m_{13} \\
&\vdots \\
h_{1k} &= h_{1(k-1)} - m_{1k}
\end{aligned} \quad (6)$$

If h_{1k} satisfies the conditions for an IMF, then h_{1k} is designated as c_1

$$c_1 = h_{1k}, \quad (7)$$

where c_1 is the first IMF component from the data. It should be noted that c_1 will contain the finest scale or the shortest period component of the signal. The next step is to remove c_1 from the rest of the data by

$$r_1 = X(t) - c_1, \quad (8)$$

where r_1 is called residue, which contains all longer period variations in the data. r_1 is treated as a new data set and subjected to the same sifting procedure described above. This procedure is repeated to all the subsequent r_j 's and will result as

$$\begin{aligned}
r_2 &= r_1 - c_2 \\
r_3 &= r_2 - c_3 \\
&\vdots \\
r_n &= r_{(n-1)} - c_n
\end{aligned} \quad (9)$$

The sifting should stop when the residue, r_n , becomes a monotonic function or a function containing only a single extrema, from which no more IMF can be extracted. Thus, the sifting process produces a decomposition of the data into n -intrinsic modes and a residue r_n

$$X(t) = \sum_{j=1}^n c_j + r_n. \quad (10)$$

When EMD method is applied, a mean or zero reference is not required; EMD needs only the locations of the local extrema. The sifting process automatically generates the zero reference for each component.

In the book by Huang and Shen ⁷⁾, the EMD was proposed as an adaptive time-frequency data analysis method and proved that it was quite flexible in a wide range of applications for extracting signals from data generated in noisy non-linear and non-stationary processes. However, one of the major drawbacks of EMD is the frequent appearance of mode mixing, which is defined as a single Intrinsic Mode Function either consisting of widely incongruent scales or a signal of similar scale residing in different IMF components. To overcome the mode mixing problem, the Ensemble Empirical Mode Decomposition was proposed.

(2) Ensemble empirical mode decomposition

Ensemble Empirical Mode Decomposition (EEMD) is a noise-assisted data analysis (NADA) method which was proposed by Wu and Huang ⁸⁾ as an improvement of the EMD. This method defines the true IMF components as the mean of an ensemble of trials where in each trial consists of the signal plus white noise of finite amplitude. Like its predecessor, EMD, this improved method separates the scale naturally without any *a priori* subjective criterion selection.

EEMD is based on the studies of the statistical properties of white noise by ^{9,10)} which showed that the EMD is an adaptive dyadic filter bank when applied to white noise, that is, the Fourier spectra of various IMFs collapse to a single shape along the axis of logarithm of period or frequency. When the data is not pure noise, some scales could be missing and that is when the mode mixing phenomenon occurs.

The principle behind EEMD is described as follows: the finite amplitude white noise added to the signal covers the whole time-frequency space uniformly with the constituting components of different scales. Although adding white noise may result in smaller signal-to-noise ratio, the added white noise serves as a uniform reference scale where the bits of the signal are automatically projected onto the proper scales to facilitate EMD. Thus, the low signal-to-noise ratio does not affect the decomposition method but actually enhances it to avoid mode mixing ⁸⁾.

(3) Hilbert spectral analysis (HSA)

Nonlinear processes need special treatment. Aside from the periodicity, the detailed dynamics in the processes from the data need to be understood well because one of the typical characteristics of nonlinear process is their intra-wave frequency modulation, which indicates the instantaneous frequency (IF) change within one oscillation cycle. As Hung *et al.* ⁸⁾ pointed out, this intra-frequency variation is the hallmark of nonlinear systems. The easiest way to obtain the instantaneous frequency is by using the Hilbert transform, through which the complex conjugate $y(t)$ of any real valued function $x(t)$ of L^P class can be determined by

$$y(t) = H[x(t)] = \frac{1}{\pi} PV \int_{-\infty}^{+\infty} \frac{x(\tau)}{t - \tau} d\tau, \quad (11)$$

where PV indicates the principal value of the singular integral. With the use of Hilbert transform, the analytic signal is defined as

$$z(t) = x(t) + iy(t) = a(t)e^{i\theta(t)}, \quad (12)$$

where

$$a(t) = \sqrt{x^2 + y^2}, \quad \text{and} \quad \theta(t) = \arctan\left(\frac{y}{x}\right). \quad (13)$$

The instantaneous amplitude is given by $a(t)$, the phase

function by $\theta(t)$, and the instantaneous frequency is given by

$$\omega(t) = \frac{d\theta(t)}{dt}. \quad (14)$$

Hilbert Spectral Analysis is a signal analysis method applying the Hilbert transform to compute the instantaneous frequency (IF) of signals according to Eq. (14). After performing the Hilbert transform on each signal, in this case the IMFs, the data can be expressed in the following form

$$z(t) = \sum_{j=1}^n a_j(t) \exp\left(i \int \omega_j(t) dt\right), \quad (15)$$

where $a_j(t)$ and $\omega_j(t)$ are the amplitude and frequency as a function of time for the j th IMF, respectively. From this expression the instantaneous frequency and amplitude as a function of time can be represented in a three-dimensional plot. This can also be represented in two dimensional plot in which the amplitude is contoured on the frequency-time plane. The frequency-time distribution of the amplitude is designated as the Hilbert Amplitude Spectrum (HAS) or simply Hilbert Spectrum (HS).

1.3 Synthetic aperture focusing technique (SAFT)

Synthetic Aperture Focusing Technique, also known as SAFT, is based on a backpropagation technique which produces an image of the object interior by focusing the recorded data. Ultrasonic SAFT imaging was originally intended for medical applications and it was adopted from optical holography and synthetic aperture imaging in radar¹¹⁾.

The SAFT algorithm numerically superimposes signals measured at several positions, thus creating a high-resolution image¹²⁾. 2-D SAFT is an integration of the time of flight (TOF) in the x-y-t data field for each element (pixel) of the specimen. It produces a two dimensional representation of the backscatter intensity from the interior of the specimen. Signals are focused to every image point and structural noise is suppressed by spatial superposition¹²⁾. It has been successfully used for imaging homogeneous materials, such as steel and aluminum, to detect and locate defects. In the case of reinforced concrete, SAFT image is expected to provide information about thickness variations as well as the inclusions such as the reinforcing bars, cracks, voids, delaminations, and deteriorated zones.

2. Methodology

2.1 Data gathering

In this study, a concrete block specimen with the following dimensions: L = 575 mm, W = 575 mm, and H = 120 mm, was used to illustrate the application of Synthetic Aperture Focusing

Technique for ultrasonic image reconstruction. The concrete specimen has a 38 mm diameter duct at the middle, with a 32 mm steel rod grouted inside as shown in Fig. 2. The ultrasonic testing apparatus consisted of the following: a high power tone burst pulser (Ritec RF Gated Amplifier), a broad band receiver (Ritec BR-640), a function generator (Agilent 33250A), a microcomputer based digital oscilloscope (Hewlett Packard Infinium Oscilloscope), and two broad band transducers with central frequency of 100 kHz (Transmitter: Japan Probe PS 936; Receiver: K GK K-85).



Fig. 2(a)



Fig. 2(b)

Fig. 1 Concrete block specimen.

(a) Pitch-Catch method conducted on the top surface of the specimen, (b) Target area for image reconstruction.

A total of 168 waveform data were recorded along a linear aperture on the top surface of the specimen by Pitch-Catch method. The position of the transmitting transducer was changed at increments of 10 mm. For each transmitter position, eight readings (four on each side) were obtained from a receiving transducer. The center-to-center distances of the transmitting and receiving transducers were 70 mm, 80 mm, 90 mm and 100 mm. The sampling frequency was set at 5.0 MSa/s (5 MHz) and obtained 1,002 data points for each waveform. The averaging method (16 waveforms) was implemented for the data acquisition in order to reduce the coherent signal noise. A band pass filter was used in order to suppress the low and high frequency vibrations. The lower and higher cut-off frequencies were at 50 kHz and 3 MHz, respectively. Moreover, the contact condition between the transducers and the concrete surface is vital to ultrasonic measurement. Aside from using a coupling gel, steel blocks were placed on top of the transducers to assure good acoustical coupling.

Before conducting the pitch-catch method, the ultrasonic velocity of the concrete block was obtained by measuring the travel time of the stress wave along a known dimension of the specimen. Using the transmitting transducer (PS 936), the ultrasonic pulse was sent to the receiving transducer (K-85) through the specimen. A cross-correlation procedure was performed between the transmitted and received signals in order

to obtain the lag time, which was used to compute for the phase velocity.

2.2 Signal processing

All of the 168 received waveforms were normalized first with respect to each individual input signals. Signal processing using Wavelet transform, Hilbert-Huang transform and combination of the two transforms were conducted to decompose the signals into simpler oscillation modes before subjecting to Synthetic Aperture Focusing Technique for image reconstruction.

(1) Wavelet transform

For Wavelet analysis, the Discrete Wavelet transform (DWT) and the Wavelet Packet transform (WPT) were conducted since the Continuous Wavelet transform (CWT) requires high computational horsepower and is not recommended for large amount of data. It should be noted that the choice of mother wavelet is very important when applying wavelet analysis to a particular problem because for a given problem, different mother wavelets will produce different results. Thus, wavelet analysis results are highly dependent on the mother wavelet, and the results are meaningful only when the chosen mother wavelet is appropriate for the problem (*a priori*). To obtain the most suitable mother wavelet for this problem, all the normalized waveform data were decomposed using different wavelets from different wavelet families such as Daubechies, Symlet, Coiflet, Biorthogonal Spline, Reverse Biorthogonal Spline and Meyer. The wavelet decomposition procedure creates approximation (cA) and detail (cD) coefficient matrices which are used to synthesized and reconstruct the waveform. The reconstructed waveforms were compared with their corresponding original waveform and error parameters such as mean absolute error (MAE), root mean squared error (RMSE) and maximum absolute error were computed. It should be noted that the smaller the error parameter value implies better decomposition-reconstruction accuracy of the wavelet.

The error parameter values for all the waveforms of each wavelet were averaged as shown in Table 1. To verify and/or support the results of Table 1, the wavelets were ranked in another method. For each of the 168 waveform data, the wavelets which gave the minimum values for each error parameter were identified and tabulated. The total number of times a particular wavelet was identified was recorded and the corresponding percentage with respect to the total number of waveforms was also computed. Then the wavelets were ranked based on their respective percentage values. Table 2 shows the top three wavelets for both the discrete wavelet transform and wavelet packet transform methods. Among all the tested wavelets, it is unanimous that the Biorthogonal of order 2.4 wavelet is the most suitable mother wavelet for processing the waveform data.

After identifying the most appropriate mother wavelet, the waveforms were subjected to discrete wavelet transform and

Table 1

Average of computed error parameter values

Wavelet Family	Order	Discrete Wavelet Transform			Wavelet Packet Transform		
		Error Parameters			Error Parameters		
		MAE	RMSE	MaxAE	MAE	RMSE	MaxAE
Daubechies	1	4.55311E-17	6.601E-17	2.964E-16	4.806E-17	6.935E-17	3.093E-16
	2	1.24619E-13	1.743E-13	6.67E-13	1.305E-13	1.813E-13	6.049E-13
	3	1.42354E-12	1.999E-12	7.029E-12	1.446E-12	2.031E-12	7.01E-12
	4	2.67685E-13	3.744E-13	1.298E-12	2.704E-13	3.783E-13	1.306E-12
	5	4.12246E-13	5.756E-13	1.977E-12	4.147E-13	5.791E-13	1.994E-12
	6	1.95275E-13	2.608E-13	8.308E-13	1.958E-13	2.617E-13	8.363E-13
	7	3.2148E-13	4.471E-13	1.516E-12	3.226E-13	4.487E-13	1.523E-12
	8	6.67881E-13	9.287E-13	3.202E-12	6.698E-13	9.314E-13	3.217E-12
	9	6.53285E-12	8.869E-12	2.818E-11	6.542E-12	8.881E-12	2.815E-11
	10	7.47141E-13	1.024E-12	3.4E-12	7.485E-13	1.026E-12	3.416E-12
Symlet	2	1.24619E-13	1.743E-13	6.67E-13	1.305E-13	1.813E-13	6.049E-13
	3	1.42354E-12	1.999E-12	7.029E-12	1.446E-12	2.031E-12	7.01E-12
	4	1.00882E-13	1.398E-13	4.81E-13	1.025E-13	1.416E-13	4.6E-13
	5	3.45142E-14	4.762E-14	1.552E-13	3.481E-14	4.8E-14	1.547E-13
	6	1.62807E-13	2.242E-13	7.422E-13	1.637E-13	2.253E-13	7.302E-13
	7	1.40712E-13	1.893E-13	5.736E-13	1.409E-13	1.896E-13	5.737E-13
	8	3.49136E-14	4.908E-14	1.636E-13	3.511E-14	4.935E-14	1.637E-13
	Coiflet	1	1.82888E-13	2.569E-13	1.102E-12	1.933E-13	2.674E-13
2	2.33911E-12	3.271E-12	1.143E-11	2.368E-12	3.309E-12	1.124E-11	
3	1.29745E-13	1.732E-13	5.255E-13	1.311E-13	1.747E-13	5.16E-13	
4	5.82211E-12	7.374E-12	2.165E-11	5.834E-12	7.387E-12	2.161E-11	
5	1.18637E-09	1.445E-09	3.604E-09	1.187E-09	1.446E-09	3.599E-09	
Biorthogonal	1.1	4.55311E-17	6.601E-17	2.964E-16	4.806E-17	6.935E-17	3.093E-16
	1.3	4.82098E-17	7.102E-17	3.277E-16	4.906E-17	7.226E-17	3.349E-16
	1.5	4.91595E-17	7.352E-17	3.456E-16	4.951E-17	7.394E-17	3.524E-16
	2.2	6.15555E-17	8.796E-17	3.691E-16	6.27E-17	8.946E-17	3.722E-16
	2.4	3.33676E-17	5.188E-17	2.681E-16	3.384E-17	5.246E-17	2.705E-16
	2.6	3.47661E-17	5.452E-17	2.841E-16	3.512E-17	5.492E-17	2.821E-16
	2.8	4.88246E-17	7.311E-17	3.436E-16	4.905E-17	7.329E-17	3.419E-16
	3.1	8.83E-17	1.242E-16	4.862E-16	9.002E-17	1.266E-16	4.943E-16
	3.3	5.43639E-17	7.937E-17	3.542E-16	5.498E-17	8.025E-17	3.562E-16
	3.5	5.48826E-17	8.026E-17	3.522E-16	5.532E-17	8.09E-17	3.553E-16
	3.7	5.82469E-17	8.519E-17	3.729E-16	5.845E-17	8.543E-17	3.751E-16
	3.9	6.08119E-17	8.965E-17	4.077E-16	6.099E-17	8.987E-17	4.084E-16
	4.4	2.11564E-13	2.957E-13	1.02E-12	2.145E-13	2.997E-13	1.021E-12
5.5	2.68331E-13	3.753E-13	1.299E-12	2.705E-13	3.784E-13	1.304E-12	
6.8	4.34271E-14	6.056E-14	2.059E-13	4.364E-14	6.085E-14	2.057E-13	
Reverse Biorthogonal	1.1	4.55311E-17	6.601E-17	2.964E-16	4.806E-17	6.935E-17	3.093E-16
	1.3	4.7561E-17	7.01E-17	3.351E-16	4.844E-17	7.134E-17	3.367E-16
	1.5	4.82991E-17	7.203E-17	3.539E-16	4.873E-17	7.267E-17	3.557E-16
	2.2	6.20993E-17	9.228E-17	3.599E-16	6.362E-17	9.328E-17	4.787E-16
	2.4	3.57796E-17	5.686E-17	3.352E-16	3.633E-17	5.745E-17	3.365E-16
	2.6	3.62518E-17	5.744E-17	3.297E-16	3.651E-17	5.77E-17	3.328E-16
	2.8	5.01444E-17	7.672E-17	4.039E-16	5.036E-17	7.698E-17	4.063E-16
	3.1	1.23803E-16	1.953E-16	1.259E-15	1.121E-16	1.697E-16	9.992E-16
	3.3	6.13742E-17	9.446E-17	4.988E-16	6.171E-17	9.484E-17	5.023E-16
	3.5	5.9251E-17	9.095E-17	4.848E-16	5.967E-17	9.144E-17	4.795E-16
	3.7	6.13061E-17	9.308E-17	4.829E-16	6.169E-17	9.36E-17	4.871E-16
	3.9	6.33215E-17	9.627E-17	5.072E-16	6.351E-17	9.653E-17	5.056E-16
	4.4	2.1174E-13	2.967E-13	1.073E-12	2.145E-13	2.997E-13	1.021E-12
5.5	2.6858E-13	3.759E-13	1.326E-12	2.705E-13	3.785E-13	1.304E-12	
6.8	4.34383E-14	6.058E-14	2.066E-13	4.364E-14	6.085E-14	2.057E-13	
Discrete Meyer		5.91571E-07	7.944E-07	2.632E-06	5.917E-07	7.946E-07	2.634E-06

Table 2

(a) Wavelet ranking based on Discrete Wavelet Transform

Rank	MAE		RMSE		MaxAE	
	wavelet	%	wavelet	%	wavelet	%
1st	bior2.4	54.2	bior2.4	57.1	bior2.4	36.9
2nd	bior2.6	26.8	bior2.6	25.0	db1	22.0
3rd	rbio2.4	13.7	rbio2.4	11.3	bior2.6	17.3

(b) Wavelet ranking based on Wavelet Packet Transform

Rank	MAE		RMSE		MaxAE	
	wavelet	%	wavelet	%	wavelet	%
1st	bior2.4	53.0	bior2.4	55.4	bior2.4	38.7
2nd	bior2.6	25.6	bior2.6	25.0	bior2.6	18.5
3rd	rbio2.4	12.5	rbio2.4	10.1	db1	17.9

wavelet packet transform using five decomposition levels. Instead of analyzing the scaleograms (time-scale-coefficient contour plot), the resulting wavelet coefficients were used to reconstruct the individual waveforms for each end node of the decomposition tree. These reconstructed sub-waveforms were

subjected to another transformation called Hilbert Transform in order to perform Hilbert Spectral Analysis (HSA). With this procedure, the spectral analysis using discrete wavelet transform, wavelet packet transform and the Hilbert-Huang transform can be compared.

(2) Hilbert-Huang transform

The normalized waveforms were subjected to Hilbert-Huang transform via empirical mode decomposition (EMD) and ensemble empirical mode decomposition (EEMD) to break down the waveforms into their basic modes of oscillation called intrinsic mode functions (IMF). After obtaining all the IMFs, the HSA procedure is applied to each IMF to obtain the instantaneous frequency (IF) and consequently the frequency-amplitude distribution as a function of time (Hilbert spectrum).

(3) Combined wavelet and Hilbert-Huang transform

Even if the EEMD method was used for Hilbert-Huang transform, there are some instances where mode mixing still occurs. In order to ameliorate this problem, it is proposed that a pre-signal processing is needed before conducting the HHT. In this paper, the wavelet packet transform was combined with Hilbert-Huang transform. The decomposition level for the WPT was set at three (3) to pre-decompose the waveform into eight (8) wavelet components. Then each of these wavelet components was subjected to HHT to further decompose them into eight (8) IMFs and a residual function.

2.3 Image reconstruction

The waveform data were evaluated through reconstruction calculations to determine the location, distribution and approximate size/dimension of acoustic reflectors and scatterers (possible defects or anomalies) in the concrete specimen being tested. In this study, the image reconstruction was done on both the processed and unprocessed waveform data for comparison.

The image reconstruction was simulated using a two-dimensional matrix, where in each pixel is in Cartesian coordinate system. The position coordinates of the transmitting (x_T, y_T) and the receiving (x_R, y_R) transducers were in accordance with the above mentioned coordinate system. Fig. 3 shows the schematic diagram for the simulation of wave propagation and reflection at a specific pixel (x_i, y_i). At a particular transmitter location, only the pixels that are located within the radiation zone of the incident wave were considered in the numerical superposition.

From the transmitting transducer, the incident wave propagates towards the pixel being considered and it is assumed that this pixel will reflect the wave towards the receiving transducers. The time of flight (TOF) is the time it takes for the signal to travel from the transmitting transducer to the pixel and from the pixel to the receiving transducer. TOF is given by the

formula

$$TOF = \frac{D_{incident} + D_{reflected}}{V}, \quad (16)$$

where

TOF : time of flight (s)

$D_{incident}$: distance or length of the incidence path (m)

$D_{reflected}$: distance or length of the reflected path (m)

V : ultrasonic velocity through the concrete specimen (m/s).

For all the recorded waveforms, the SAFT algorithm numerically superimposes the amplitude value corresponding to the computed TOF to the specific pixel (x_i, y_i) as given by Eq. (17). This procedure is done for all the pixels within the radiation zone. The summation of the amplitude values will result in an image wherein a pixel with high intensity indicates the location of a reflector (or possible defect).

$$S(x_i, y_i) = \sum_{n=1}^N A_n(TOF) \quad (17)$$

where

$S(x_i, y_i)$: summation of amplitude values for pixel i

$A_n(TOF)$: amplitude value of the n^{th} waveform corresponding to the computed TOF

N : total number of recorded waveform data

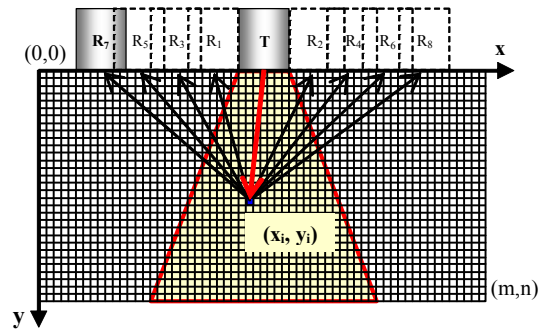


Fig. 3 Schematic diagram for 2D Pitch-Catch SAFT.

3. Results and discussion

The waveforms obtained from the eight (8) receiver positions at a particular transmitter location were normalized with respect to the input waveform. Fig. 4 shows the normalized waveforms at the location where the transmitter is directly above the embedded steel rod. It can be observed that each of these waveforms contains a lot of oscillations, making it very difficult to analyze and interpret. A SAFT image using all the 168 normalized waveforms is shown in Fig. 5. The reflection from the bottom surface of the concrete specimen is not clearly depicted from the reconstructed image. Moreover, the grouted steel rod cannot be located from this SAFT image. Thus, processing the waveforms is necessary to obtain better and

meaningful images.

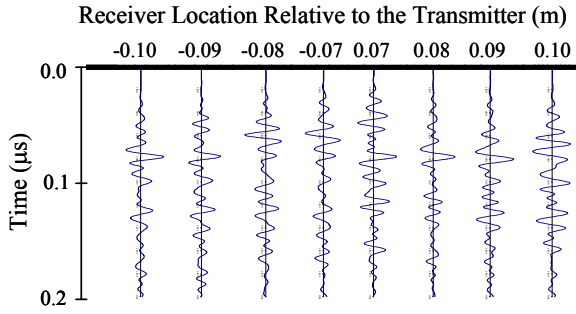


Fig. 4 Normalized waveforms.

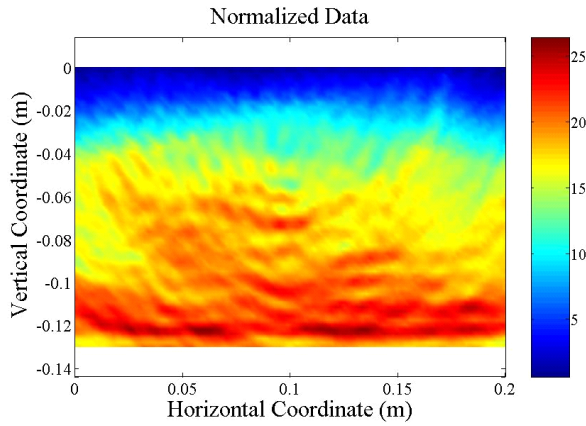


Fig. 5 SAFT image of normalized data.

The signal processing methods decompose the waveforms into several components. For instance, the discrete wavelet transform (DWT) with five decomposition levels breaks down each of the normalized waveform into an approximation (A) and five (5) details (D). Referring to Fig. 1(a), A and D are numbered from 1 to 5 in accordance to the decomposition level number. For the case of the wavelet packet transform (WPT), two decomposition levels were used in this study: three and five. Using three decomposition levels, it will break down the signal into eight (8) decomposition components while for the case of five decomposition levels, the signal will be decomposed into thirty two (32) components. Referring to Fig. 1 (b), these components are numbered based on their node index. For example, the first and last decomposition components for WPT level 3 are labeled as N(3,0) and N(3,7), respectively. On the other hand, Hilbert-Huang transform (HHT), for both EMD and EEMD, the signals were decomposed into eight (8) intrinsic mode functions (IMF) and a residual function (R). Furthermore, when the 3-level WPT is combined with the HHT, the number of resulting decomposition components becomes seventy two (72). The WPT initially decomposes the waveform into eight (8) wavelet components and then each of these components was further decomposed into eight (8) IMFs and a residual function.

All of the decomposition components were used for SAFT imaging. However, in order to decide which waveform decomposition components from each signal processing methods

will be used for the image comparison, the correlation coefficient of the decomposed signal with each individual decomposition components were computed and ranked accordingly. All the waveforms were normalized first with respect to their maximum absolute values before taking the correlations. In this way, all the decomposition components are analyzed on the same grounds. That is, even the waveforms with small energy components can still be included in the image comparison. From each signal processing methods, the top four (4) decomposition components with the highest average correlation coefficients are considered and compared in this paper. Table 3 shows the top four decomposition components from each signal processing methods.

Table 3

Average correlation coefficient for each decomposition component

Signal Processing	Decomp. Comp.	Ave. Corr. Coeff.
DWT(L5)	DWT: A5	0.682190
	DWT: D5	0.678911
	DWT: D4	0.279553
	DWT: D3	0.039391
WPT(L3)	N(3,0)	0.999356
	N(3,1)	0.039391
	N(3,3)	0.002503
	N(3,2)	0.002487
WPT(L5)	N(5,0)	0.682190
	N(5,1)	0.678911
	N(5,3)	0.254436
	N(5,2)	0.135151
HHT(EMD)	IMF-1	0.889785
	IMF-2	0.426593
	IMF-3	0.075103
	IMF-4	0.015496
HHT(EEMD)	IMF-4	0.852368
	IMF-3	0.789634
	IMF-5	0.441596
	IMF-6	0.097629
WPT(L3)-HHT(EMD)	N(3,0) IMF-1	0.737885
	N(3,0) IMF-2	0.435114
	N(3,3) IMF-4	0.182919
	N(3,1) IMF-3	0.182619
WPT(L3)-HHT(EEMD)	N(3,0) IMF-4	0.870232
	N(3,0) IMF-3	0.791282
	N(3,1) IMF-4	0.535480
	N(3,0) IMF-5	0.447164

One of the 168 normalized waveforms used in this study is shown in Fig. 6, as well as its corresponding frequency spectrum. It can be observed that the signal have very strong frequency components in the range of 50 to 150 kHz, however, weak frequency components of up to 1.5 MHz are also present.

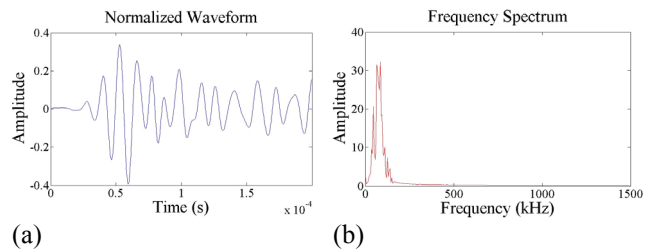


Fig. 6 Normalized waveform (a) and its corresponding frequency spectrum (b).

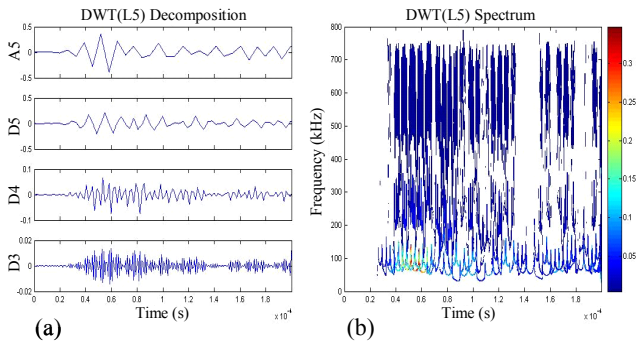


Fig. 7 DWT (Level 5) decomposition. (a) Top 4 decomposition components, (b) Hilbert spectrum.

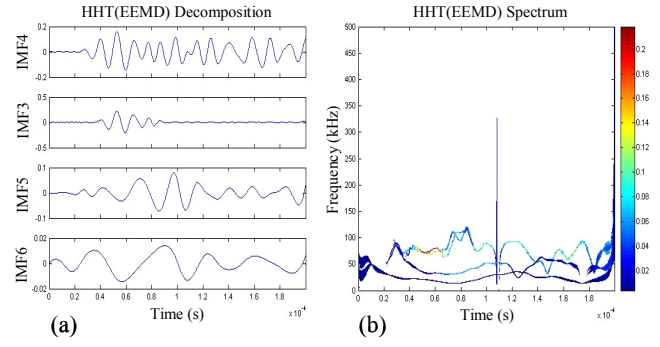


Fig. 11 HHT (EEMD) decomposition. (a) Top 4 decomposition components, (b) Hilbert spectrum.

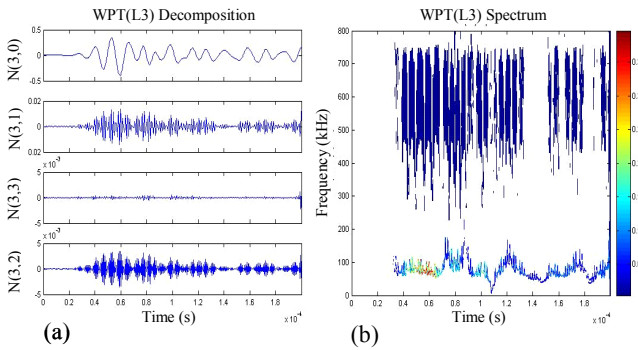


Fig. 8 WPT (Level 3) decomposition. (a) Top 4 decomposition components, (b) Hilbert spectrum.

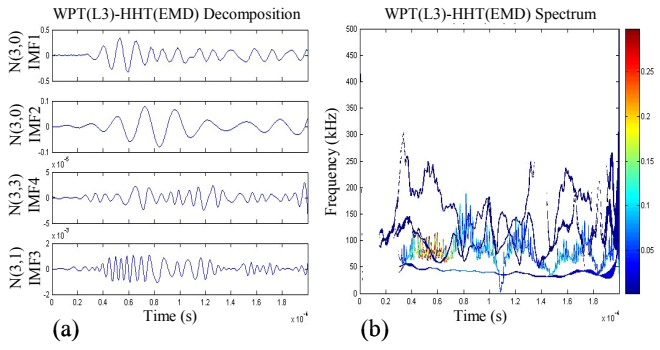


Fig. 12 WPT (L3)-HHT (EMD) decomposition. (a) Top 4 decomposition components, (b) Hilbert spectrum.

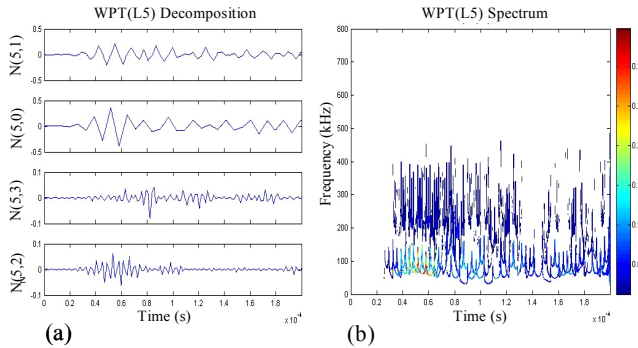


Fig. 9 WPT (Level 5) decomposition. (a) Top 4 decomposition components, (b) Hilbert spectrum.

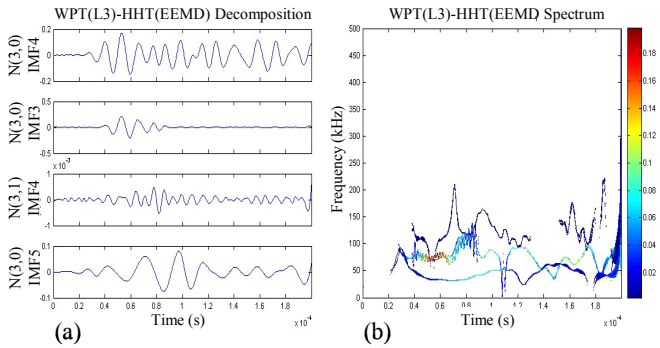


Fig. 13 WPT (L3)-HHT (EEMD) decomposition. (a) Top 4 decomposition components, (b) Hilbert spectrum.

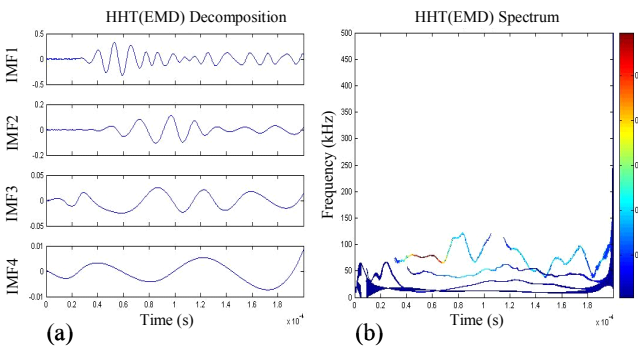


Fig. 10 HHT (EMD) decomposition. (a) Top 4 decomposition components, (b) Hilbert spectrum.

Fig. 7 to 13 show the top four (4) decomposition components, based on correlation coefficients, from each signal processing method. Also, the Hilbert spectrum (time-frequency-amplitude contour plots) for each decomposition components are shown on the right portion of these figures.

It is interesting to note that for the wavelet decompositions, DWT (Fig. 7) and WPT (Fig. 8 and Fig. 9), the resulting wavelet decomposition components have sharp peaks and are very erratic, particularly the detail components. As a consequence, the instantaneous frequencies (Hilbert spectrum) are not narrow band and changes very rapidly. It can be observed that the top two

decomposition components (top 1 and top 2) have frequency range approximately from 50 to 150 kHz while the other two components (top 3 and top 4) have higher frequency ranges. Unlike the wavelet results, the Hilbert-Huang transform decomposition results (Fig. 10 and Fig. 11) are smooth primarily because of the iteration procedure which involves getting the cubic spline of the extremum values. It is important to notice the order on how the decomposition components are arranged according to rank. Recall that the decomposition via EMD or EEMD is from the component with highest frequency down to the component with lowest frequency (monotonic). In Fig. 10 (a), IMF 1, which is the top 1 in the rank, has the highest frequency among the IMF components and it is followed by IMF 2, IMF 3 and IMF 4, which are arranged in decreasing frequency. However, in Fig. 11 (a), the top in the ranking is IMF 4 and then followed by IMF 3, IMF 5 and IMF 6. Note that IMF 1 and IMF 2 contain very high frequency components corresponding to the white noise added during the EEMD procedure, hence both have very low correlation coefficients. Also, from the Hilbert spectrum shown in Fig 10 (b) and Fig. 11 (b), it can be observed that the instantaneous frequencies are well localized. However, there are instances where the instantaneous frequencies of different intrinsic modes functions overlap. This is one of the drawbacks of HHT, the occurrence of mode mixing.

As mentioned above, the top four decomposition components from each signal processing methods are used for comparing the images reconstructed via synthetic aperture focusing technique (SAFT). The reconstructed images for each signal processing methods are shown in Fig. 14 to 20. It should be noted that the pixels with high intensity (colored in red) indicate locations of reflectors. However, it should be emphasized that when comparing these images, the scale values corresponding to the color scales, found at the right side of each images, be taken into consideration.

Looking at the top left images of Fig. 14, Fig. 15 and Fig. 16, produced by the discrete wavelet transform and the wavelet packet transform, all of these images show the location of the concrete bottom surface as well as the grouted steel rod. However, it can be observed that unlike the bottom surface (concave part) of the steel rod, the top surface (convex part) is not clearly visible. Also, it can be seen that the region between these two surfaces is shaded by color blue, indicating very low reflection intensity. This low intensity region pertains to the homogeneous interior of the steel rod. In addition, it can be observed that signal processing using wavelets produce a single image (image (a) in Figs. 14 to 16) that shows the reflection from the concrete bottom surface and the reflections from the top and bottom surfaces of the steel rod. It is also worth noticing that images (c) and (d), which correspond to the decomposition components with frequencies higher than 150 kHz, does not represent clear physical meaning. Thus, it is important to consider the Hilbert spectrum when interpreting the reconstructed SAFT images.

Comparing the images shown in Fig. 15(a) and Fig. 16(a), it seems that the WPT level 3 image is better than that of WPT level 5 in terms of the reflection intensity for the top and bottom surface of the steel rod. In connection with this, it can also be observed that the corresponding (b), (c) and (d) images for both levels have large differences in reflection intensities, primarily because the signals were decomposed into different number of components, thirty two components for WPT level 5 while there are only eight components in WPT level 3. Thus, WPT level 3 gives clearer and higher reflection intensity image based on the first decomposition component but it did not give much decomposition details in the succeeding wavelet component images.

Comparing the images from the two HHT decomposition methods, EMD and EEMD, it is obvious that the EEMD gives better images than EMD. Also, EEMD was able to produce separate images for the reflection from the concrete bottom surface and the reflections from the grouted steel rod. It can be observed in Fig. 18(a) that the image of the steel rod is well manifested by strong reflection intensities from the top and bottom surfaces and very low reflection intensity from its interior. Again, it should be noted that the low reflection intensity in that region simply signifies that the interior of the grouted steel rod is relatively homogeneous compared to the surrounding concrete. In addition, the bottom surface of the concrete specimen is well defined by the high reflection intensity pixels located approximately 0.12 m from the top surface as shown in Fig. 18(b). From these observations, it also follows that the corresponding images from WPT(Level3)-HHT(EEMD) are far better than the images produced by WPT(Level3)-HHT(EMD) as shown in Fig. 20 and Fig. 19, respectively. Moreover, comparing Fig. 20 and Fig. 18, it can be observed that combining WPT(Level3), as a pre-signal processing method, with HHT(EEMD) slightly improves the images given by HHT(EEMD) alone. That is, the reflector locations, concrete

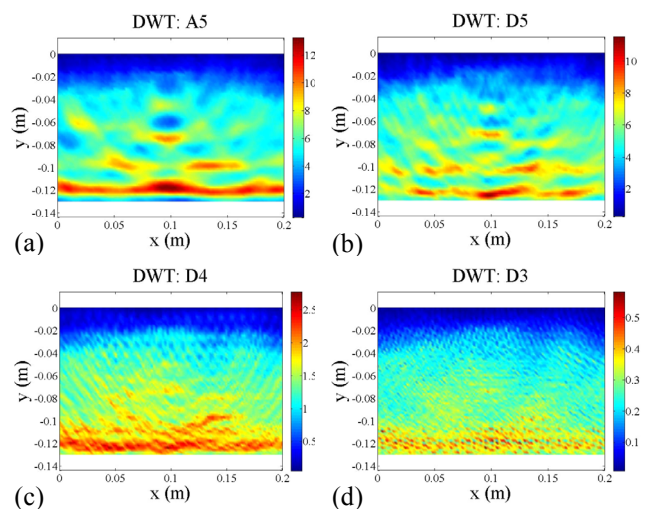


Fig. 14 SAFT images based on DWT (Level 5) decomposition. (a) A5, (b) D5, (c) D4, (d) D3.

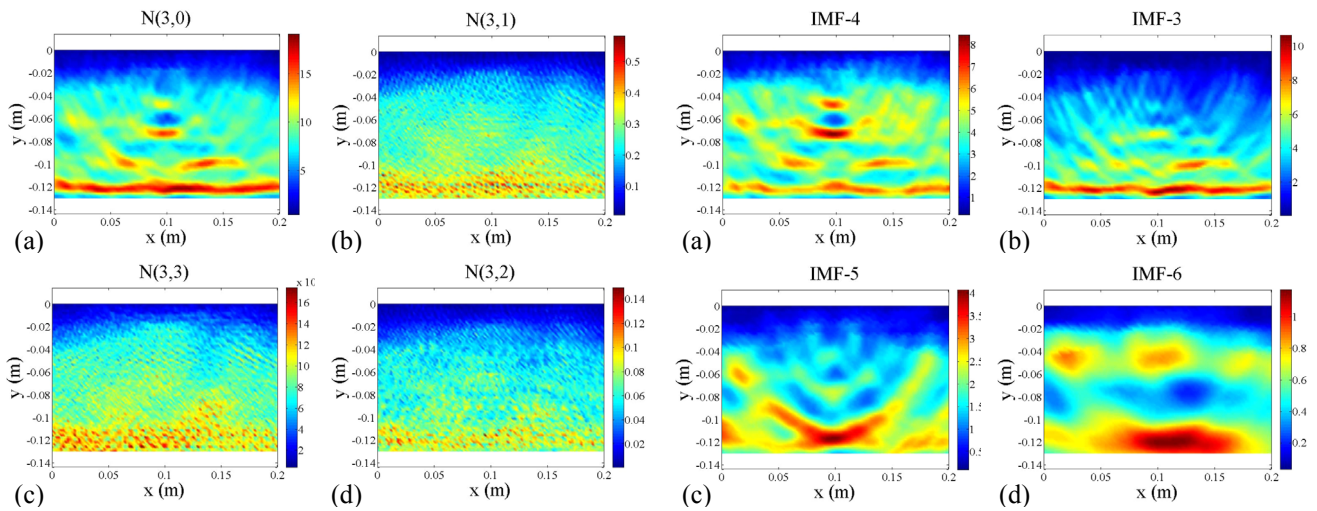


Fig. 15 SAFT images based on WPT (Level3) decomposition. (a) N(3,0), (b) N(3,1), (c) N(3,3), (d) N(3,2).

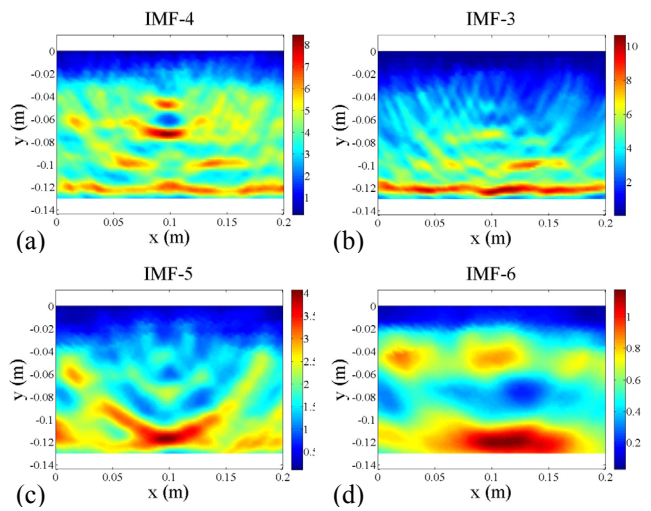


Fig. 18 SAFT images based on HHT (EEMD) decomposition. (a) IMF-4, (b) IMF-3, (c) IMF-5, (d) IMF-6.

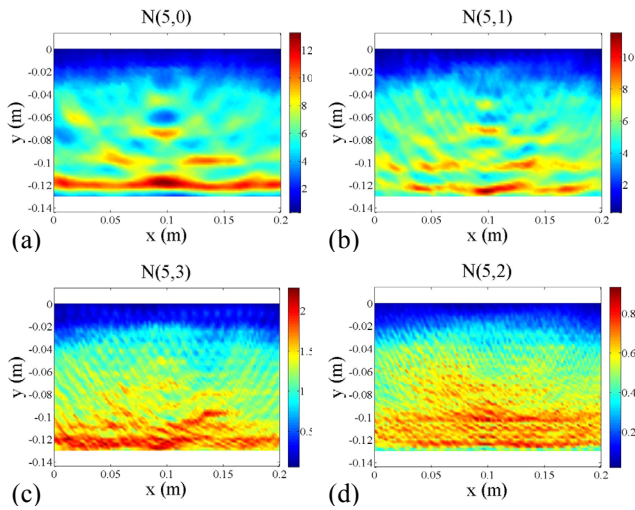


Fig. 16 SAFT images based on WPT (Level5) decomposition. (a) N(5,0), (b) N(5,1), (c) N(5,3), (d) N(5,2).

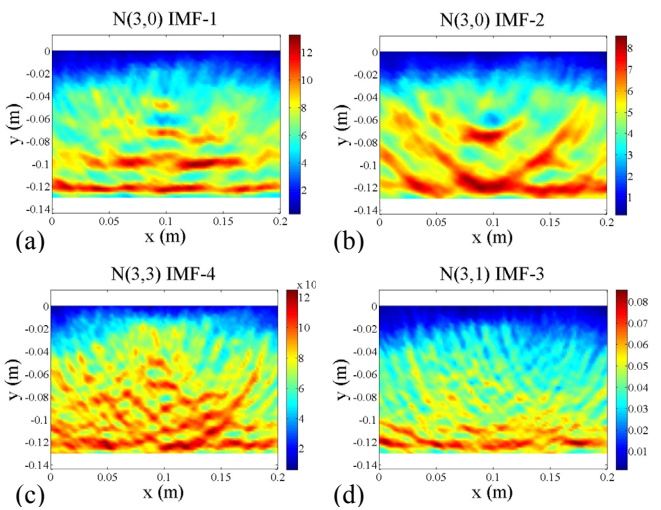


Fig. 19 SAFT images based on WPT (Level3)-HHT (EMD) decomposition. (a) N(3,0) IMF-1, (b) N(3,0) IMF-2, (c) N(3,3) IMF-4, (d) N(3,1) IMF-3.

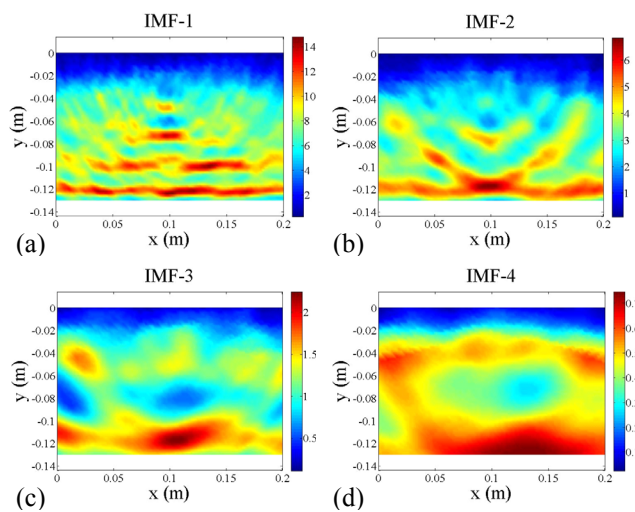


Fig. 17 SAFT images based on HHT (EMD) decomposition. (a) IMF-1, (b) IMF-2, (c) IMF-3, (d) IMF-4.

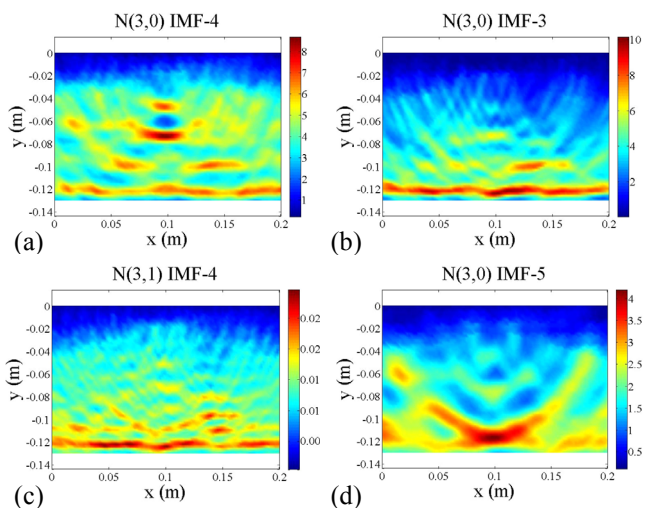


Fig. 20 SAFT images based on WPT (Level3)-HHT (EEMD) decomposition. (a) N(3,0) IMF-4, (b) N(3,0) IMF-3, (c) N(3,1) IMF-4, (d) N(3,0) IMF-5.

bottom surface and the top and bottom surfaces of the steel rod, are more emphasized. These pixel locations have higher reflection intensities relative to the other surrounding pixels. This can be verified by comparing the maximum values in the reflection intensity scales found at the right portion of each image. Also, Table 3 shows that the average correlation coefficients for the corresponding top four decomposition components of WPT(Level3)-HHT(EEMD) are larger than that of HHT(EEMD). Moreover, the former gives an additional image of the concrete bottom surface due to waveforms with low energy components as shown in Fig. 20(c).

4. Conclusion

In this paper, all of the 168 received waveforms were first normalized with respect to each individual input signals. The Synthetic Aperture Focusing Technique was used to obtain the image of the concrete specimen, however it did not give a meaningful image result. Thus, the need for signal processing prior to SAFT imaging is necessary. Signal processing using Wavelet transform, Hilbert-Huang transform and the proposed combination of the two transforms were conducted to decompose the signals into simpler oscillation modes before subjecting to SAFT for image reconstruction. The resulting images from each signal processing methods were compared. All the methods were able to show the locations of the concrete bottom surface as well as the top and bottom surfaces of the grouted steel rod. However, the proposed method, WPT-HHT(EEMD), gave the best image results. Also, it was able to show the reflections from the concrete bottom surface and the steel rod surfaces into separate images. WPT serves as a preprocessor to decompose the original signal into narrow band signals and then further decomposed using the EEMD in order to obtain the IMFs and residual function. It is necessary to apply a selection criteria to eliminate the undesirable components and retain the meaningful ones. Since the superposition of all IMFs and residual function represents the original signal, the relevant components should have strong correlation with the original signal while the irrelevant components should have weak correlation. Therefore, since the components are separated from each other and the irrelevant components are eliminated, the accuracy in arrival time extraction is greatly improved.

It is important to reiterate that wavelet analysis results are highly dependent on the mother wavelet, and the results are meaningful only when the chosen mother wavelet is appropriate for the problem (*a priori*). Unlike wavelet analysis, the Hilbert-Huang analysis is adaptive. Being adaptive means that the definition of the basis function has to be data-dependent, an *a posteriori*-defined basis, so that the IMFs can reflect the physical properties of the original data.

Finally, anomaly or defect detection in concrete structures through ultrasonic imaging was greatly improved by the combination of WPT-HHT as signal processing methods, and SAFT as an imaging tool. Moreover, an efficient and accurate evaluation of the concrete structure interior was made possible with these combined techniques.

Acknowledgement

In this paper, The authors would like to thank Dr. Norden E. Huang, Dr. Zhaohua Wu and Mr. Seng-Chung Su for the help in understanding the implementation of HHT. Also, the principal author would like to thank the Japan Society for the Promotion of Science (JSPS) and the Japanese Government (MEXT) for providing scholarship for his graduate studies at Tokyo Institute of Technology.

REFERENCES

- 1) Buyukozturk ,O.: Imaging of concrete structures, *NDT&E International*, Vol. 31, No. 4, pp.233-243, 1998.
- 2) Repair-Evaluation-Maintenance-Rehabilitation Research Program, REMR Technical Note CS-ES 1.10, 1991.
- 3) Proakis, J.G. and Manolakis, D.G.: *Introduction to Digital Signal Processing*, Macmillan, New York, 1988.
- 4) MATLAB [computer software]. *The Math Works, Inc.*
- 5) Abbate, A., DeCusatis, C. M. And Das, P. K.: *Wavelets and Subbands Fundamentals and Applications*, Birkhauser, Boston, 2002.
- 6) Huang, N. E., Shen, Z., Long, S. R, Wu, M. C., Shih, H..H, Zheng, Q., Yen, N. C., Tung, C. C. and Liu, H. H.: The empirical mode decomposition and the Hilbert spectrum for nonlinear and non-stationary time series analysis, *Proc. R. Soc. London, Ser. A*, 454, pp. 903-995, 1998.
- 7) Huang, N. E. and Shen, S. S. P.: *Hilbert-Huang Transform and Its Applications*, World Scientific Publishing Co. Pte. Ltd., Singapore, 2005.
- 8) Wu, Z. and Huang, N. E.: Ensemble empirical mode decomposition, *Advances in Adaptive Data Analysis*, Vol. 1, No. 1, pp.1-41, 2009.
- 9) Flandrin, P., Rilling, G. and Goncalves, P.: Empirical mode decomposition as a filter bank, *IEEE Signal Process. Lett.* **11**, pp.112-114, 2004.
- 10) Wu, Z. and Huang, N. E.: A study of the characteristics of white noise using the empirical mode decomposition method, *Proc. Roy. Soc. Lond. Ser. A*460, pp.1597-1611, 2004.
- 11) Flaherty, J. J, Erikson, K. R. and Lund, V. M.: Synthetic aperture ultrasound imaging systems, United States Patent, US 3,548,642, 1970.
- 12) Schickert, M. M. K. and Muller, W.: Ultrasonic imaging of concrete elements using reconstruction by synthetic aperture focusing technique, *Journal of Materials in Civil Engineering* © ASCE, pp.235-246, 2003.

(Received: March 9, 2010)